# A SIMPLE AIRCRAFT FUEL SYSTEM MODEL FOR CENTER OF GRAVITIY ESTIMATION

E. Özger,
Technische Hochschule Ingolstadt, 85049 Ingolstadt, Germany

**Abstract**

Agile, high performance aircraft are based more and more on flight mechanical unstable airframes with control laws stabilizing the air vehicle. It requires among others an accurate knowledge of the center of gravity position, particularly during agile maneuvering. Thus, this investigation is intended to serve a systematic framework in form of a fuel system which tries to cover all aspects of defueling during flight and which is formulated as a state space model. Measurement and process noise as well as biases are accounted for in the performance characteristics of fuel pumps and fuel probes. A simple maneuver simulation delivers the rates and accelerations exerted on the tanks which are typical for maneuvering. Various approaches such as an output and stabilized output error approach are compared with a simulated fuel probe measurement with respect to their fuel state prediction capability where all of them do not show the necessary reliability. Main outcome is that an open unguided integration of nominal pump rates as done in the output error method will not give acceptable results due to the presence of process and measurement noise. Stabilizing this method with measurement information improves the accuracy but still shows drawbacks particularly for lateral cg because the introduced measurement information is not fully harmonized with the time integration of the nominal pump rates which does not account the presence of process and measurement noise and any biases. Probe data gives robust fuel state information with average accuracy but still lacks the required local accuracy when content rates and fuel inclination angle increase at half empty tank contents. Thus, all approaches fail to provide the necessary accuracy particularly during maneuvering conditions so that future works must focus on approaches which can fuse all available sensor and fuel system information in an optimal way.

## 1. INTRODUCTION

This investigation deals with the problem of center of gravity (c.g.) calculation for maneuvering aircraft based on the fuel state estimation within the various tanks which are drained according to a certain fuel management logic. The c.g. position depends very much on the knowledge of the fuel content in the tanks. The main requirements on the fuel system comprise safe fuel provision of the engines during all possible flight conditions and failure cases. The accurate knowledge where the fuel is situated at any instant does not normally have the highest priority in the requirement list of a fuel system. There are various investigations on fuel slosh (Gangadharan et al. [1]), particularly for space vehicles, or estimation of fuel consumption from flight path in order to optimize the ATC traffic (Yendler et al. [2], Trani et al. [3], Collins et al. [4]), which is not the focus of this investigation.

Modern aircrafts nowadays optimize more and more the flight performance by influencing the c.g. towards the aft position, thus destabilizing the airframe. This requires control laws to stabilize the aircraft. One major prerequisite for the manipulation of the c.g. is the accurate knowledge of its position. To achieve this, the fuel system comprises fuel probes within the tanks which give an estimate of the fuel content. Also the massflow through the fuel pumps can be integrated to obtain the consumed and remaining fuel amount. Both measurement devices and approaches are normally not optimized to give very accurate estimates of the fuel content during a whole mission.

Normally, a set of fuel probes are located within the tank which is flat and irregularly formed to fit in the free space of the wing or the fuselage. Therefore, the measurement accuracy of the fuel probes depend heavily on the flight condition e.g. cruise flight or agile maneuvering. This leads to a certain fuel distribution within the tank volume which is sometimes more or less measurable. Fuel probe measurement and integration of pump rates may have different fuel state prediction characteristics depending on the acceleration on the tank, the fuel consumption and fuel content.

Comparable to the task of flight path reconstruction where different sensor source information is fused into one synchronized picture, the fuel state within the tanks can also be reconstructed by the sensor information of the fuel probes and fuel pumps. The aim of this paper is to introduce a fuel system model which will serve as frame work for future work which will focus on reconstructing the fuel states with an accurate and robust approach. To accomplish this, a theoretical simulation model of an aircraft fuel system model with all relevant features which are necessary to analyze the performance of the fuel probes and fuel pumps is introduced. It is assumed that the measurement capability of the devices is average and only partly known so that the necessity and the effect of the reconstruction approach can be shown.

This paper starts by describing the fuel system in all its relevant aspects where the technical side is presented together with a theoretical foundation in form of a state space model. Then, an overview is given where the

measurement and simple estimation approaches of fuel probe and fuel pump rate fail to give an accurate estimate of the fuel content and therefore center of gravity position.

## 2. MOTIVATION

This investigation is based on a generic fighter aircraft (15to MTOW) with twin engines shown in figure 1. The aircraft geometric data is summed up in Table 1. The c.g. position is located aft of the aerodynamic center in order to give better agility and flight performance. In order to get an overview on the influence between c.g. position and flight mechanical requirement a simple investigation of the time to double $T_2$ is performed by equations (1) to (5). The linearized equations of motion for a short period motion are used to give the eigenvalue $\lambda$ which is a function of the force $Z_\alpha$, stability $M_\alpha c_{m\alpha}$ and damping $M_q$, $c_{mq}$ derivatives that depend on dynamic pressure $p_{dyn}$, velocity $V_0$, earth acceleration $g$, wing area $S$, wing chord $c$, trim lift coefficient $c_{A0}$, mass $m$, Inertia around y axis $I_y$. Stability and damping derivatives $M_\alpha$, $M_q$ of the aircraft are built up by the wing (subscript *wing*) and horizontal stabilizer (subscript *hst*) contributions which are calculated together with lever arm $x_{CG}$ (distance between 25% wing and c.g.) and the lever arm $r_N$ between wing and horizontal stabilizer. The pitching moment contribution of the lift of wing and horizontal stabilizer are assumed at their ¼ lines. For this the unstable, positive real valued eigenvalue $\lambda$ of the short period oscillation is computed by means of the normal force and pitching moment characteristics based on the assumption that both wing and horizontal stabilizer produce lift linearly with angle of attack $\alpha$. Figure 2 shows that for a c.g. shift of 5cm ($x_{CG}$ = -1.15m→-1.2m) due to the defueling process the time to double $T_2$ may change dramatically ($T_2$ = 2.8s → 1.4s). Therefore, the flight control system and control laws must know at any instant where exactly the c.g. is in order to stabilize the aircraft appropriately.

(1) $$T_2 = \frac{\ln(2)}{\lambda} \quad \text{with}$$

(2) $$\lambda = \frac{Z_\alpha + M_q}{2} + \sqrt{\left(\frac{Z_\alpha + M_q}{2}\right)^2 + M_\alpha - Z_\alpha M_q}$$

(3) $$Z_\alpha \approx -\frac{p_{dyn}\cdot S\cdot c_{A0}}{m\cdot V_0},\ p_{dyn} = \frac{\rho}{2}V_0^2,\ c_{A0} = \frac{m\cdot g}{p_{dyn}S}$$

(4) $$M_q \approx 2\frac{p_{dyn}\cdot S\cdot c^2\cdot c_{mq}}{I_y\cdot V_0} = -2\frac{p_{dyn}\cdot S\cdot c^2}{I_y\cdot V_0}\left(c_{A\alpha,wing}\left(\frac{x_{CG}}{c}\right)^2 + c_{A\alpha,hst}\left(\frac{x_{CG}+r_N}{c}\right)^2\frac{S_{hst}}{S}\right)$$

(5) $$M_\alpha \approx 2\frac{p_{dyn}\cdot S\cdot c\cdot c_{m\alpha}}{I_y\cdot V_0} = 2\frac{p_{dyn}\cdot S\cdot c}{I_y\cdot V_0}\left(-c_{A\alpha,wing}\left(\frac{x_{CG}}{c}\right) - c_{A\alpha,hst}\left(\frac{x_{CG}+r_N}{c}\right)\frac{S_{hst}}{S}\right)$$

## 3. MODEL OF AIRCRAFT FUEL SYSTEM

The fuel system of a generic fighter aircraft with 15to MTOW with two engines (comparable to an Fairchild Republic A-10) consists of left and right hand wing tank, as well as a forward and aft central tank situated in the fuselage part (see figure 1). Each engine is fed by the wing tank at its side by an engine pump. The wing tanks itself are provided with fuel by the forward and aft central tanks by means of a forward and aft pump that feed a galley. The wing tanks are connected to the galley by valves which allow transfer to the tank only if opened. Each tank is equipped with fuel probes that measure approximately the content. The tank geometry and position information for all four tanks is summarized in Table 2.

### 3.1. Flight Mechanics Simulation

In order to keep the level of complexity as low as necessary the flight mechanics simulation is based on the body fixed accelerations $A_{AC} = (N_X, N_Y, N_Z)^T$ and angular rates $\omega=(p, q, r)^T$ given in body fixed coordinates as a function of time with time step $n$. Numeric integration of these values gives the velocity in body fixed coordinates $V_{AC}$. The acceleration in earth fixed coordinates $A_{Earth} = d^2X_E/dt^2$, Euler angles $(\Phi,\Theta,\Psi)^T$, earth fixed flight velocity $V_{Earth} = dX_E/dt$, earth fixed position $X_E$ are determined by the transformation matrix $M_{Earth2AC}$ and successive integrations (see equations (6) to (12)).

(6) $$\frac{\vec{V}_{AC}^{\,n} - \vec{V}_{AC}^{\,n-1}}{\Delta t} = g\cdot\begin{pmatrix}N_X(t)\\N_Y(t)\\N_Z(t)\end{pmatrix} - \begin{pmatrix}p(t)\\q(t)\\r(t)\end{pmatrix}\times\vec{V}_{AC}^{\,n-1} \rightarrow \vec{V}_{AC}^{\,n}$$

(7) $$M_{Earth2AC} = \begin{pmatrix}1 & 0 & 0\\0 & \cos\Phi & \sin\Phi\\0 & -\sin\Phi & \cos\Phi\end{pmatrix}\cdot \begin{pmatrix}\cos\Theta & 0 & -\sin\Theta\\0 & 1 & 0\\\sin\Theta & 0 & \cos\Theta\end{pmatrix}\cdot \begin{pmatrix}\cos\Psi & \sin\Psi & 0\\-\sin\Psi & \cos\Psi & 0\\0 & 0 & 1\end{pmatrix}$$

(8) $$\vec{V}_{Earth} = \int\vec{A}_{Earth}dt \rightarrow \vec{X}_{Earth} = \int\vec{V}_{Earth}dt$$

(9) $$\frac{d\vec{V}_{Earth}}{dt} = \vec{A}_{Earth} = M_{Earth2AC}^T\cdot\vec{A}_{AC},\ \vec{A}_{AC} = \begin{pmatrix}N_X\\N_Y\\N_Z\end{pmatrix}\cdot g$$

(10) $$M_{Euler} = \begin{pmatrix}1 & \sin\Phi\tan\Theta & \cos\Phi\tan\Theta\\0 & \cos\Phi & -\sin\Phi\\0 & \sin\Phi/\cos\Theta & \cos\Phi/\cos\Theta\end{pmatrix}$$

(11) $$\begin{pmatrix}\dot\Phi & \dot\Theta & \dot\Psi\end{pmatrix}^T = M_{Euler}^T\cdot\vec{\omega},\ \vec{\omega} = \begin{pmatrix}p & q & r\end{pmatrix}^T$$

(12) $$\int\begin{pmatrix}\dot\Phi & \dot\Theta & \dot\Psi\end{pmatrix}^T dt = \begin{pmatrix}\Phi & \Theta & \Psi\end{pmatrix}^T$$

Climb angle $\gamma$ is calculated by equation (13) and angle of attack $\alpha$ and angle of sideslip $\beta$ with equation (14) and (15).

(13) $\gamma = -\arcsin\left(\frac{V_{z,Earth}}{|V_{Earth}|}\right)$

(14) $\alpha = \arctan\left(\frac{V_{z,AC}}{V_{x,AC}}\right)$

(15) $\beta = \arctan\left(\frac{V_{y,AC}}{\sqrt{V_{x,AC}^2 + V_{z,AC}^2}}\right)$

The acceleration at the tanks $A_{Tank}$ must be computed from the aircraft acceleration $A_{AC}$, the angular rate $\omega$ = ($p$, $q$, $r$)$^T$ and acceleration $d\omega/dt$ and the distance between aircraft cg position $R_{AC}$ and tank position $R_{Tank}$ (see Table 2) which is shown by equation (16).

(16) $\vec{A}_{Tank} = \vec{A}_{AC} + \vec{\omega} \times \left(\vec{\omega} \times \left(\vec{R}_{Tank}^{CG} - \vec{R}_{AC}^{CG}\right)\right) + \dot{\vec{\omega}} \times \left(\vec{R}_{Tank}^{CG} - \vec{R}_{AC}^{CG}\right)$

Furthermore, the acceleration rate $S_{Tank}$ at the tank is computed by equation (17).

(17) $\vec{S}_{Tank} = \dot{\vec{A}}_{Tank} + \vec{\omega} \times \vec{A}_{Tank}$

### 3.2. State Space Fuel System Model

The mathematical representation of a state space model for the fuel model can be summarized as follows

(18) $\vec{x}(t) = \left(x_{LHW} \quad x_{RHW} \quad x_{FWD} \quad x_{AFT}\right)^T$

(19) $\vec{u}(t) = \left(L_{EngLH} \quad L_{EngRH}\right)^T$

(20) $\dot{\vec{x}}(t) = \vec{f}\left(\vec{x}(t), \vec{u}(t), \vec{z}(t), \vec{\theta}\right) + F \cdot \vec{w}(t)$

(21) $\vec{z} = \vec{g}\left(\vec{x}, \vec{\vartheta}\right) + G \cdot \vec{v}(t)$ where

(22) $\vec{z} = \vec{z}(t) = \left(z_{LHW} \quad z_{RHW} \quad z_{FWD} \quad z_{AFT}\right)^T$

Here $x$ is the fuel state vector describing the true fuel content of the four tanks, $t$ is the time, $u$ is the known control input vector describing the engine power setting, $z$ is the measured fuel state vector, $f$ and $g$ are the non-linear system state and observation functions, $\theta$ is the vector of unknown parameters for the fuel states, $\vartheta$ is the vector of unknown parameters for the measured fuel state, $F$ is the process noise distribution matrix, $G$ is the measurement noise distribution matrix, $w$ is the process noise, and $v$ is the measurement noise both with variance 1.

### 3.3. Fuel System State Function *f* and Process Noise *F·w*

The functioning of the fuel system, which can be seen as the defueling sequence, is described in the state function $f$. The defueling sequence is separated into various fuel stages $FS$ depending on the content of the tanks, as described by Table 3.

As can be seen, the wing tanks are drained first until they reach 70% of maximum tank content (FS=0). Then, fuel is provided from the forward tank to the galley by the forward pump until the forward tank reaches 50% content (FS=1). In the next step the aft tank supports the galley until both central tanks are empty ($FS=2$ and $FS=3$). In the last stage ($FS=4$) the wing tanks are drained until they are emptied. Fuel can enter the wing tanks only if its corresponding valve is opened which happens if the wing tank content is below 70%. This means that fuel is transferred from the central to the wing tanks maintaining a wing tank content of 70% until the central tanks are empty. In case that both wing tanks receive fuel from the galley the distribution, how much the left and right tanks obtain, is quantified by the distribution factors $\lambda_{LH}$ and $\lambda_{RH}$, which are modeled as a function of the difference of left to right wing tank fuel content. If one of the wing tank contents is above 70% the fuel of the galley is transferred only to the other one which is quantified by the fuel states $FS=11/12/21/22/31/32$. The true fuel pump rates $p^{True}$ and their corresponding process noise $Fw$ are modeled in equation (23) to (26). It is assumed that the true pump rate $p^{True}$ depend on the nominal or demand pump rate $p_{Nom}$ and linearly on the tank content as well as the fuel inclination angle $\tau$, which is calculated as angle between the tank acceleration vector $A_{Tank}$ and the normal vector of the tank $(0\ 0\ -1)^T$. The stochastic contribution of the true pump rate is modeled by the process noise $Fw$. The process noise $Fw$ itself depends on the tank content $x$ and on the fuel inclination angle $\tau$. The process noise consists of two contributions, namely the basic inaccuracy $F_1$ of the fuel pump rate and the variations $F_2$ due to fuel inclination angle $\tau$ (see equation (25)).

(23) $p^{True} = p_{Nom} + \frac{\partial p}{\partial x}\left(x - p_0 \cdot x_{\max}\right) + \frac{\partial p}{\partial \tau}\frac{\tau}{\pi} + F \cdot w(t)$

(24) $\tau = \arccos\left(\frac{\vec{A}_{Tank} \cdot (0 \quad 0 \quad -1)^T}{|\vec{A}_{Tank}|}\right)$

(25) $F_2^2(x,\theta) = \frac{l_1}{0.8^2}\min\left(1 - \frac{x}{x_{\max}}, 0.8\right)^2\left(l_2 + 1 - \exp\left[-\left(\frac{\tau}{\sigma_\tau}\right)^2\right]\right)$

(26) $F_{Tank} = \sqrt[4]{F_1^4 + F_2^4}$

The pump rate dependency on tank content $\partial p/\partial x$ and on fuel inclination angle $\partial p/\partial \tau$, the process noise contributions $F_1$ and $F_2$ and the distribution factor $\lambda$ of fuel between left and right tanks are summarized in Table 4.

The vector of unknown parameters of the fuel states $\theta$ is a bias and represents a non-stochastic deviation of the true pump rate from the nominal or demand value $p_{Nom}$. The bias $\theta$ is a function of fuel state $x$ and fuel inclination angle $\tau$ and comprises the fuel distribution factor $\lambda_{LH}$ as shown in equation (27).

The process noise distribution matrix $F$ is modeled according to equation (28) where the Gaussian white noise vector $w$ is produced by a random number generator with variance 1 independently for each tank.

(27) $$\vec{\theta} = \begin{pmatrix} \frac{\partial p_{LHW}}{\partial x_{LHW}} \\ \frac{\partial p_{LHW}}{\partial \tau_{LHW}} \\ \frac{\partial p_{RHW}}{\partial x_{RHW}} \\ \frac{\partial p_{RHW}}{\partial \tau_{RHW}} \\ \frac{\partial p_{FWD}}{\partial x_{FWD}} \\ \frac{\partial p_{FWD}}{\partial \tau_{FWD}} \\ \frac{\partial p_{AFT}}{\partial x_{AFT}} \\ \frac{\partial p_{AFT}}{\partial \tau_{AFT}} \\ \lambda_{LH} \end{pmatrix}$$

(28) $$F = \begin{pmatrix} F_{LHW} & 0 & 0 & 0 \\ 0 & F_{RHW} & 0 & 0 \\ 0 & 0 & F_{FWD} & 0 \\ 0 & 0 & 0 & F_{AFT} \end{pmatrix}$$

### 3.4. Fuel System Observation Function *g* and Measurement Noise *G·v*

The fuel probe measurement performance is described in the observation function *g* where it is assumed that the fuel probes within one tank are not able to determine exactly the fuel content. The measured value *z* deviates from the true fuel content *x* by a non-stochastic and stochastic contribution which are the bias $\vartheta$ and the measurement noise *Gv (*see equation (29)). Thus, the measured value *z* comprises besides the true content value *x,* a bias $\vartheta$ and the measurement noise *Gv* modeled as Gaussian white noise contribution *G·v*. The Gaussian white noise vector *v* with variance 1 is produced by a random number generator independently for each tank.

(29) $$\vec{z} = \vec{x} + \vec{\vartheta} + G \cdot \vec{v}$$

The bias $\vartheta$ and measurement noise *G·v* depend on the fuel content *x*, the fuel content rate *dx/dt,* the fuel inclination angle $\tau$ and the rate of acceleration at the tank *S*. The measurement noise distribution matrix *G* is modeled accordingly by means of four terms $G_1$, $G_2$, $G_3$, $G_4$ for each tank.

(30) $$G_1^2(x) = k_1^2 \max\left(\frac{x}{x_{\max}}, 0.3\right)^2 \exp\left[-\left(\frac{x - x_{\max}}{\sigma_1}\right)^2\right]$$

(31) $$G_2^2(x) = k_1^2 \max\left(\frac{x}{x_{\max}}, 0.3\right)^2 \left(1 - \exp\left[-\left(\frac{\dot{x}}{\sigma_2}\right)^2\right]\right)$$

(32) $$G_3^2(x, \theta) = k_1^2 \max\left(\frac{x}{x_{\max}}, 0.3\right)^2 \left(k_2 + 1 - \exp\left[-\left(\frac{\tau}{\sigma_3}\right)^2\right]\right)$$

(33) $$G_4^2(x, S) = k_1^2 \max\left(\frac{x}{x_{\max}}, 0.3\right)^2 \left(k_3 + 1 - \exp\left[-\left(\frac{|\vec{S}_{Tank}|}{\sigma_4}\right)^2\right]\right)$$

The measurement noise distribution matrix is formed according to

(34) $$G = \begin{pmatrix} G_{LHW} & 0 & 0 & 0 \\ 0 & G_{RHW} & 0 & 0 \\ 0 & 0 & G_{FWD} & 0 \\ 0 & 0 & 0 & G_{AFT} \end{pmatrix}$$ with

(35) $$G_{Tank} = \sqrt[4]{G_1^4 + G_2^4 + G_3^4 + G_4^4}$$

Since the acceleration at each tank may differ from each other the measurement distribution matrix can have different element values. Table 5 summarizes the parameter values used in equation (30) to (33). The bias vector $\vartheta$ quantifies the systematic and non-stochastic unknown measurement error of the fuel probes, which is modeled in equation (36). The error is modeled as a time dependent sine wave with frequency and phase which depend on the measurement noise elements G of the corresponding tanks. This measurement error is meant to model the dynamic liquid behavior of the fuel which will lead to a systematic erroneous measurement of the fuel content.

(36) $$\vec{\vartheta} = \begin{pmatrix} -G_{LHW} \sin\left(2\pi \frac{t}{10 \cdot G_{LHW}} + 10 \frac{\pi}{180} G_{LHW}\right) \\ -G_{RHW} \sin\left(2\pi \frac{t}{10 \cdot G_{RHW}} + 10 \frac{\pi}{180} G_{RHW}\right) \\ -G_{FWD} \sin\left(2\pi \frac{t}{10 \cdot G_{FWD}} + 10 \frac{\pi}{180} G_{FWD}\right) \\ -G_{AFT} \sin\left(2\pi \frac{t}{10 \cdot G_{AFT}} + 10 \frac{\pi}{180} G_{AFT}\right) \end{pmatrix}$$

### 3.5. Inertia Model

The following equation (37) is used to compute the total aircraft c.g. position $R_{AC}$ out of zero fuel mass & cg $m_0$, $R_0$, the tank c.g. position ($R_{LHW}$, $R_{RHW}$, $R_{FWD}$, $R_{AFT}$) and fuel content information ($x_{LHW}$, $x_{RHW}$, $x_{FWD}$, $x_{AFT}$)

(37) $$\vec{R}_{AC}^{CG} = \frac{\begin{pmatrix} \vec{R}_0^{CG} m_{Zero} + \vec{R}_{LHW}^{CG} x_{LHW} + \vec{R}_{RHW}^{CG} x_{RHW} \\ + \vec{R}_{FWD}^{CG} x_{FWD} + \vec{R}_{AFT}^{CG} x_{AFT} \end{pmatrix}}{m_{Zero} + x_{LHW} + x_{RHW} + x_{FWD} + x_{AFT}}$$

The c.g. of each tank is based on the acceleration vector $A_{Tank}$ at each tank which gives the fuel inclination angle ($\phi_{Tank}, \theta_{Tank}$), the fuel content *x* and its dimensions length $L_L$ and width $L_W$. Normally, this modeling can be derived easily by 3D CAD programs. Since such a program was not available for the author, an approximate model for the c.g. derivation is assumed as summarized in equation (38) and (39). The positions of the tanks $R_{Tank}$ are given in Table 2. The zero fuel c.g. is at $\vec{R}_0^{CG} = \begin{pmatrix} -1.2m & 0 & 0 \end{pmatrix}^T$

with a zero fuel mass of $m_{Zero}$ = *10to*.

$$(38)\quad \vec{R}_{Tank}^{CG} = \vec{R}_{Tank} + \frac{1}{4}\left(1-\cos\left(2\pi\frac{x}{x_{\max}}\right)\right)\begin{pmatrix} L_L \sin(\theta_{Tank}) \\ L_W \sin(\phi_{Tank}) \\ 0 \end{pmatrix}$$

with

$$(39)\quad \theta_{Tank} = \arctan\left(\frac{A_{x,Tank}}{A_{z,Tank}}\right), \phi_{Tank} = \arctan\left(\frac{A_{y,Tank}}{A_{z,Tank}}\right)$$

## 4. FUEL SYSTEM SIMULATION

In the following, the fuel states are determined by means of the simulation model which is presented in chapter 3. The true fuel states are compared with the simulated fuel probe values, the estimates of the fuel states based on an output error (OE) and on a stabilized output error (SOE) approach. Two types of maneuvers are flown, namely a steady and level flight around *-1g* (negative z-direction = lift direction) and a dynamic maneuver between *-5g to 4g*.

The output error (OE) approach represents basically the nominal fuel run down. It is determined by integrating the nominal pump rates $p_{Nom}$ without the bias vectors ($\vartheta,\theta$) across the nominal fuel stages nor the process and measurement noise contributions (*F,G*). The fuel stages during defueling are therefore nominal ones. The stabilized output error method (SOE) also does not account for the bias vectors ($\vartheta,\theta$) and the process and measurement noise contributions (*F,G*) but the integration is guided by the true fuel stage information during defueling. Therefore, the deviations during defueling may not be as large as for the OE approach. The fuel probe information is presented by three values, minimum (*ProbeMin*), maximum (*ProbeMax*) and mean value (*ProbeMean*). Minimum and maximum fuel probe values are evaluated by determining the lower and upper envelope values of the noisy fuel probe data. The mean value corresponds to the average value of the upper and lower envelope.

### 4.1. Fuel System Simulation during S&L Flight

Figures 3 to 10 and Tables 6 to 10 summarize the results of the fuel system simulation for a steady level flight (S&L). In Figure 3 to 6 the fuel content of the left and right wing tanks ($x_{LHW}$,$x_{RHW}$) as well as the content of the forward and aft tanks ($x_{FWD}$,$x_{AFT}$) are shown. Figure 7 gives an overview of the nominal (OE) and true fuel stages during the simulation and Figure 8 shows the content rates dx/dt for the tanks. CG information is summarized in Figures 9 and 10 for longitudinal and lateral cg position. The simulation lasts for 1150sec ≈ 20 minutes and shows the true, measured and estimated defueling processes. The nominal defueling process which is represented by the output error approach (OE) is characterized by the defueling of the wing tanks until they reach 70% of tank content (fuel stage *FS=0* until *T≈60sec*). Fuel is then transferred from forward tank to the wing tanks so that the wing tanks hold on to 70% and until the forward tank is drained to 50% (fuel stage *FS=1* until *T≈330sec*). After that, further fuel is provided both by the forward and aft tanks until the forward tank is empty (fuel stage *FS=2* until *T≈650sec*). In *FS=3* the forward tank is empty and only the aft tank supports the wing tanks (until *T≈900sec*). In the last fuel stage *FS=4* the remainder of the wing tanks are emptied (see also Figure 7 for fuel stage overview as a function of time). In the nominal defueling process no asymmetries in the wing are evident. After T=1050sec all fuel is nominally consumed whereas the true defueling process shows that there are 400kg in the wing tanks. The true defueling shows that the fuel stages 2,3 and 4 occur earlier and last longer than nominally. Moreover, asymmetric conditions in the wing tanks (*FS=11/12/21/22/31/32*) due to the process noise and the wing distribution factors $\lambda_{LH}$ and $\lambda_{RH}$ are evident. The true pump rates deviate from the nominally defined ones due to the fuel content in the tanks $\partial p/\partial x$ and the process noise *F* showing a higher pumping rate when draining the central tanks in *FS=2,3* and a lower pump rate when draining the wing tanks in *FS=4*. Figure 8 shows that the pump rate may reach values up to *dx/dt* = 11kg/s. The measured fuel contents which are shown by the probe values are conservative in the sense that they tend to show lower content values than the true ones. Tables 6 to 10 summarize these characteristics where the output error approach show deviations in the tank content up to 583kg as maximum value and ±290kg as RMS value. This means translated into a deviation of the cg position that the longitudinal cg differs from the true values up to $\Delta x_{CG}$ = *0.2m* locally and $\Delta x_{CG}$ = *±0.082 m* in average and a lateral cg deviation of $\Delta y_{CG}$ = *0.005m* locally and $\Delta y_{CG}$ = *±0.002 m* in average (see also Figures 9 and 10 for cg information as a function of time).

The stabilized output error method (SOE) shows a better performance where the maximum tank content deviation is maximum 105kg with an RMS value of ±62kg which translates to lower deviations in the longitudinal cg position of up to $\Delta x_{CG}$ = *0.021m* locally and $\Delta x_{CG}$ = *±0.01 m* in average and laterally of up to $\Delta y_{CG}$ = *0.019m* locally and $\Delta y_{CG}$ = *±0.01* in average. The worse performance in predicting the lateral cg position comes from the fact that the fuel stages are taken from the true measured ones though there may be still fuel within the tanks due to the nominal pump rates of the method. The lateral cg position reacts more sensitive to this drawback of the method. Here, the overall problem of the stabilization is that the switching from one fuel state to the other is forced by measurement data and not by the correct fuel contents. Therefore, the unused fuel contents contribute in an accumulated way to the deviations.

The minimum probe data (*ProbeMin*) has a maximum deviation in tank content of 152kg with an average value of ±80kg which amounts to maximum longitudinal cg deviation of $\Delta x_{CG}$ = *0.029m* and an average RMS value of $\Delta x_{CG}$ = *±0.008,* and laterally a deviation of $\Delta y_{CG}$ = *0.028m* locally and $\Delta y_{CG}$ = *±0.004 m* in average. The maximum probe data (*ProbeMax*) shows a maximum deviation in tank content of 87kg with an average value of ±30kg which amounts to maximum longitudinal cg deviation of $\Delta x_{CG}$ = *0.025m* and an average RMS value of $\Delta x_{CG}$ = *±0.006,* and laterally a deviation of $\Delta y_{CG}$ = *0.014m* locally and $\Delta y_{CG}$ = *±0.003 m* in average. The mean probe data (*ProbeMean*) has a maximum deviation in tank content of 96kg with an average value of ±34kg which amounts to maximum longitudinal cg deviation of $\Delta x_{CG}$ = *0.018m* and an average RMS value of $\Delta x_{CG}$ = *±0.004,* and laterally a deviation of $\Delta y_{CG}$ = *0.014m* locally and $\Delta y_{CG}$ = *±0.002 m* in average.

The probe data shows the best performance in determining the tank contents and derive the cg position,

at least for straight and level flight though its deviation may also account up to $\Delta x_{CG}$ = *0.018m* which is a non-negligible error on the time to double characteristics. Then, the SOE approach is the most promising next candidate but it fails predicting the lateral cg position since adopting the true fuel states does not lead to the correct fuel contents in the tank when using the nominal instead of the true pump rate behavior.

### 4.2. Fuel System Simulation during Maneuvering

In order to evaluate the performance of the fuel system under dynamic conditions a maneuver is proposed whose Euler angles ($\Phi,\Theta,\Psi$), angular rates ($p,q,r$) and accelerations ($dp/dt,dq/dt,dr/dt$), translational acceleration ($A_x,A_y,A_z$) and acceleration rates ($S_x,S_y,S_z$), flow ($\alpha,\beta$) and flight path $\gamma$ angles, fuel inclination angle $\tau$ as well as the maneuver path ($X_E$) is shown in Figures 11 to 23. The maneuver starts with a short $A_Z$ = *-4g* turn (~50sec) and a straight segment with dynamically changing accelerations up to $A_Z$ = *-5g* (~600sec) and is concluded with a longer turning motion at $A_Z$ = *-4g* (~100sec), see Figure 11 for the flight path. Angular rates ($p,q,r$) are changing between ±25°/s (Figure 13) with angular accelerations ($dp/dt,dq/dt,dr/dt$) up to 250°/s², see Figure 12. Bank and pitch angle ($\Phi,\Theta$) are below ±50°. Maximum accelerations in x- and y-direction $A_x,A_y$ are usually within ±1g but can reach values up to $A_x$ = 2.5g and $A_y$ = 5g at the tanks (see Figures 18 and 19). The normal acceleration varies between $A_Z$ = -5g and 3g (see Figure 20) where straight and level flight has a normal acceleration of $A_Z$ = -1g. Acceleration rates vary usually between $S_X$ = ±50g/s, $S_Y$ = 60g/s and $S_Z$ = 50g/s where some peak values above 120g/s are possible, see Figures 21 to 23. Angle of attack $\alpha$ changes between +50° and -20°, angle of sideslip $\beta$ stays within ±20° and flight path angle is around $\gamma$ = ±5° (see Figure 16) with aircraft velocity $V_{AC}$ between 80kts and 220kts (Figure 15). Fuel inclination angle $\tau$ at the tanks may reach values of up 170° (see Figure 17).

Deviations of fuel content from true value in the tanks are summarized in Table 6 to 10 and Figures 26 to 29 for the measured and estimated values. The fuel stage information as function of time is shown in Figure 24 and the content rates of the tanks are given in Figure 25. The largest deviations in fuel content can be seen again in the output error approach (OE), see Table 6, where maximum error can reach up to $\Delta x_{AFT}$ = 843kg in the aft tank with an average error of up to $\Delta x_{AFT}$ = ±373kg as RMS value. This can be translated as longitudinal cg error of $\Delta x_{CG}$ = -0.31m as peak value and $\Delta x_{CG}$ = ±0.101m as RMS value, whereas the lateral error can reach peak values of up to $\Delta y_{CG}$ = 0.142m and $\Delta y_{CG}$ = ±0.017m as average RMS value. Figures 30 and 31 show the deviations in the cg position for the probe values and estimates with OE and SOE. The OE method deviates in the longitudinal and lateral cg especially when FS = 20 and 30 is reached that is when forward and aft tanks are drained to support the wing tanks. Due to the unmodelled asymmetries in the fuel distribution factor $\lambda_{LH}$ and $\lambda_{RH}$ the lateral cg motion cannot be represented correctly. Compared with S&L flight, the dynamic maneuver produces deviations to the true values for the OE approach which are 50% higher in the longitudinal cg position and over ten times higher for the lateral cg position.

The stabilized output error method (SOE) shows the largest deviations in the tank content with $\Delta x_{AFT}$ = 269kg at an average RMS value of $\Delta x_{AFT}$ = ±106kg, see Table 7, which is an increase of two to three times the values of the S&L flight. This leads to a four times higher error in longitudinal cg position as peak value ($\Delta x_{CG}$ = -0.093m), and two times higher error in the RMS value ($\Delta x_{CG}$ = ±0.024m). Also the lateral cg shows almost three times higher deviations in the peak value ($\Delta y_{CG}$ = 0.053m) and same values in the RMS value ($\Delta y_{CG}$ = ±0.01m) compared to S&L flight. The insufficient stabilization as described in chapter 4.1 is therefore aggravated locally due to the larger off-nominal pump rate conditions during maneuvering compared to straight and level flight.

Minimum, maximum and mean probe data (*ProbeMin, ProbeMax, ProbeMean*) show in Table 8 to 10, that the peak tank content values show deviations up to two times higher compared to S&L flight whereas their RMS values do almost not change compared to S&L flight. The longitudinal cg position may deviate two to three times the value during S&L flight for the peak and RMS values (e.g. for *ProbeMean*, peak: $\Delta x_{CG}$ = 0.055m / RMS: $\Delta x_{CG}$ = ±0.009m). The lateral cg position may deviate two to four times (peak: $\Delta y_{CG}$ = -0.079m / RMS: $\Delta x_{CG}$ = ±0.005m) value during S&L flight for the peak and RMS values.

For all discussed approaches be it OE, SOE or probe values the increased angular and translational accelerations in the maneuver lead to a worsening of the prediction capability for the tank contents of two to four times the value for S&L flight and subsequently to a higher error in predicting the cg position of two to four times for the RMS value and even higher values when considering peak values.

Compared among each other the OE approach shows the worst prediction capability since the integration of nominal pump rates without accounting for any unmodelled effect or noise lead to large deviations in tank content and cg position. Providing further fuel stage information makes the SOE approach more robust where the cg prediction capability becomes two to three times better compared to the OE approach but still with significant deviations in peak values. A slightly better approach is to use probe data where RMS data show a much better cg prediction capability but with worse performance considering the peak values, especially for the lateral cg position. It is also interesting to note that the performance worsening of the SOE and probe approaches take place at different conditions. For longitudinal and lateral cg position the probe data shows a worse performance when *FS=10* and *FS=22* whereas the SOE approach worsens when *FS=20* and *FS=32*. The reason can be found in the content rate of the forward tank which starts to be drained when *FS=2* is reached in order to support the wing tanks. The accelerated decrease in tank content worsens the measurement capability of the probes which can be seen in the term $G_2$ especially when the tank is half empty. The SOE approach suffers also from pump rate deviations from the nominal value which comes into play for larger fuel inclination angles $\tau$ and when the fuel pressure due to the tank content forces the pumps to work at off-nominal conditions. This effect for the SOE approach worsens at the end of the integration time when the errors accumulate more and more.

## 5. CONCLUSION

This investigation presents a fuel system model for a fighter aircraft together with a simple maneuver simulation in order to understand the prediction capability of various methods applied such as an output error method, a stabilized output error method and simulated probe measurements. The fuel system simulation, formulated as a state space model, covers a variety of influencing stochastic and non-stochastic factors which may deteriorate the measurement and estimation capability of the above mentioned methods. Among these influences are unmodelled pump rates which are a function of the fuel inclination angle and tank content as well as an unknown in the fuel distribution between left and right wing tank. The probe measurements are worsened by the tank content, its rate, the fuel inclination and the acceleration rate at the tanks. Each of the factors serve as unknown bias in the state and observation equations as well as modeling term in the process and measurement noise formulation.

This state space model is applied for a steady and level flight and a dynamic maneuver in order to show the prediction performance of the methods, the conditions when they start to worsen and also to compare among them. An open integration approach such as the output error method fails to predict the fuel content and subsequently the cg position because process and measurement noise effects together with unmodelled non-stochastic biases let the predicted values differ considerably from the true ones. Stabilizing the method with measurement data improves the accuracy but still shows unacceptable large errors in fuel content and cg position locally which may accumulate at the end of the integration process. Furthermore, introducing measurement data does only partly improve drawbacks in prediction capability due to process and measurement noise since switching from one fuel state to the other is not triggered by the correct fuel state but forced deliberately.

Probe measurements pose the most robust approach to predict fuel content and cg position in average since no time integration is involved. But still significant local deviations in peak values for fuel content and cg position are present, which come from higher fuel content rates and fuel inclination angles which are normally present during agile maneuvering.

Therefore, this approach is intended to develop a robust method in the future which may reconstruct the fuel states and the cg position more reliably. This may be performed by a filter error method that can handle process and measurement noise as well as estimate the unknowns which are not tackled within this investigation. The fuel system model may have inaccuracies compared with complex fuel systems of high performance aircraft nowadays but the effects which form the stochastic and non-stochastic unknowns are widely comprised even if the modeling numbers may be subject to change. Therefore this investigation is also intended to give the engineer a tool in order to survey sensitivities of such a complex fuel model and test the best possible methodology to construct the fuel states which will lead to more reliable cg estimations.

## 6. REFERENCES


[1] Gangadharan, S., Sudermann, J., Marlowe, A., Njenga, C., „Parameter Estimation of Spacecraft Fuel Slosh Model",presented in the 45th AIAA/ASME/ASCE/AHS/ASC Structures, Structural Dynamics & Materials Conference, April 2004, AIAA-2004-1965

[2] Yendler, B., Lawson, W., Cheuvront, A., McAllister G., "Fuel Estimation for Stardust-NExT Mission", presented in the AIAA Space2010 Conference and Exhibit, August 2010, AIAA-2010-8712.

[3] Trani, A., Wing-Ho, F., Schilling, G., Baik, H., "A Neural Network Model to Estimate Aircraft Fuel Consumption", presented in the AIAA 4th ATIO Forum, September 2004, AIAA-2004-6401.

[4] Collins, B., P.,"Estimation of Aircraft Fuel Consumption", Journal of Aircraft, Vol. 19, No. 11, November 1982, pp. 969-975


## 7. TABLES

| Density $\rho$ | Wing Area S | Horizontal Stabilizer Area $S_{hst}$ | Chord c | Distance Wing to Stabilizer $r_N$ | Speed $V_0$ | Lift Gradient $c_{A\alpha,wing}$ and $c_{A\alpha,hst}$ | Mass m | Inertia $I_y$ |
|---|---|---|---|---|---|---|---|---|
| *1.2 kg/m³* | *64m²* | *10m²* | *4m* | *8m* | *80m/s = 155KTS* | *2$\pi$* | *12to* | *10000kgm²* |

**Table 1.** Aircraft data

| Tank | Maximum Content [kg] | Position x/y/z [m] $R_{Tank}$ | Width/Length/Height [m] |
|---|---|---|---|
| Left Wing Tank | 1000 | -1/-3.5/0 | 4/2/0.156 |
| Right Wing Tank | 1000 | -1/3.5/0 | 4/2/0.156 |
| Forward Tank | 1500 | 3.5/0/0 | 1/3/0.625 |
| Aft Tank | 1500 | -5.5/0/0 | 1/3/0.625 |

**Table 2.** Tank geometry information

| FS | Triggering Condition | Defueling Sequence | Pump Rates |
|---|---|---|---|
| 0 | $z_{LHW}, z_{RHW} \geq 70\%$ | $\dot{x}_{LHW} = p^{0}_{LHW}, \dot{x}_{RHW} = p^{0}_{RHW},$ $\dot{x}_{FWD} = \dot{x}_{AFT} = 0$ | $p^{0}_{LHW} = -p^{True}_{LHW} \cdot L_{EngLH}$ $p^{0}_{RHW} = -p^{True}_{RHW} \cdot L_{EngRH}$ |
| 10 | $z_{LHW}, z_{RHW} < 70\%$ $\wedge$ $z_{FWD} > 50\%$ | $\dot{x}_{LHW} = p^{10}_{LHW}, \dot{x}_{RHW} = p^{10}_{RHW},$ $\dot{x}_{FWD} = p^{10}_{FWD}, \dot{x}_{AFT} = 0$ | $p^{10}_{LHW} = -p^{True}_{LHW} \cdot L_{EngLH} + \lambda_{LH} p^{True}_{FWD}$ $p^{10}_{RHW} = -p^{True}_{RHW} \cdot L_{EngRH} + \lambda_{RH} p^{True}_{FWD}$ $p^{10}_{FWD} = -p^{True}_{FWD}$ |
| 11 | $z_{LHW} < 70\% \wedge$ $z_{RHW} \geq 70\% \wedge$ $z_{FWD} > 50\%$ | $\dot{x}_{LHW} = p^{11}_{LHW}, \dot{x}_{RHW} = p^{11}_{RHW},$ $\dot{x}_{FWD} = p^{11}_{FWD}, \dot{x}_{AFT} = 0$ | $p^{11}_{LHW} = -p^{True}_{LHW} \cdot L_{EngLH} + p^{True}_{FWD}$ $p^{11}_{RHW} = -p^{True}_{RHW} \cdot L_{EngRH}$ $p^{11}_{FWD} = -p^{True}_{FWD}$ |
| 12 | $z_{LHW} \geq 70\% \wedge$ $z_{RHW} < 70\% \wedge$ $z_{FWD} > 50\%$ | $\dot{x}_{LHW} = p^{12}_{LHW}, \dot{x}_{RHW} = p^{12}_{RHW},$ $\dot{x}_{FWD} = p^{12}_{FWD}, \dot{x}_{AFT} = 0$ | $p^{12}_{LHW} = -p^{True}_{LHW} \cdot L_{EngLH}$ $p^{12}_{RHW} = -p^{True}_{RHW} \cdot L_{EngRH} + p^{True}_{FWD}$ $p^{12}_{FWD} = -p^{True}_{FWD}$ |
| 20 | $z_{LHW}, z_{RHW} < 70\%$ $\wedge$ $z_{FWD} \leq 50\%$ | $\dot{x}_{LHW} = p^{20}_{LHW}, \dot{x}_{RHW} = p^{20}_{RHW},$ $\dot{x}_{FWD} = p^{20}_{FWD}, \dot{x}_{AFT} = p^{20}_{AFT}$ | $p^{20}_{LHW} = -p^{True}_{LHW} \cdot L_{EngLH} + \lambda_{LH}\left(p^{True}_{FWD} + p^{True}_{AFT}\right)$ $p^{20}_{RHW} = -p^{True}_{RHW} \cdot L_{EngRH} + \lambda_{RH}\left(p^{True}_{FWD} + p^{True}_{AFT}\right)$ $p^{20}_{FWD} = -p^{True}_{FWD},\ p^{20}_{AFT} = -p^{True}_{AFT}$ |
| 21 | $z_{LHW} < 70\% \wedge$ $z_{RHW} \geq 70\% \wedge$ $z_{FWD} \leq 50\%$ | $\dot{x}_{LHW} = p^{21}_{LHW}, \dot{x}_{RHW} = p^{21}_{RHW},$ $\dot{x}_{FWD} = p^{21}_{LHW}, \dot{x}_{AFT} = p^{21}_{AFT}$ | $p^{21}_{LHW} = -p^{True}_{LHW} \cdot L_{EngLH} + p^{True}_{FWD} + p^{True}_{AFT}$ $p^{21}_{RHW} = -p^{True}_{RHW} \cdot L_{EngRH}$ $p^{21}_{FWD} = -p^{True}_{FWD},\ p^{21}_{AFT} = -p^{True}_{AFT}$ |
| 22 | $z_{LHW} \geq 70\% \wedge$ $z_{RHW} < 70\% \wedge$ $z_{FWD} \leq 50\%$ | $\dot{x}_{LHW} = p^{22}_{LHW}, \dot{x}_{RHW} = p^{22}_{RHW},$ $\dot{x}_{FWD} = p^{22}_{FWD}, \dot{x}_{AFT} = p^{22}_{AFT}$ | $p^{22}_{LHW} = -p^{True}_{LHW} \cdot L_{EngLH}$ $p^{22}_{RHW} = -p^{True}_{RHW} \cdot L_{EngRH} + p^{True}_{FWD} + p^{True}_{AFT}$ $p^{22}_{FWD} = -p^{True}_{FWD},\ p^{22}_{AFT} = -p^{True}_{AFT}$ |
| 30 | $z_{LHW}, z_{RHW} < 70\%$ $\wedge$ $z_{FWD} \leq 0.01\%$ | $\dot{x}_{LHW} = p^{30}_{LHW}, \dot{x}_{RHW} = p^{30}_{RHW},$ $\dot{x}_{FWD} = 0, \dot{x}_{AFT} = p^{30}_{AFT}$ | $p^{30}_{LHW} = -p^{True}_{LHW} \cdot L_{EngLH} + \lambda_{LH} p^{True}_{AFT}$ $p^{30}_{RHW} = -p^{True}_{RHW} \cdot L_{EngRH} + \lambda_{RH} p^{True}_{AFT}$ $p^{30}_{AFT} = -p^{True}_{AFT}$ |
| 31 | $z_{LHW} < 70\% \wedge$ $z_{RHW} \geq 70\% \wedge$ $z_{FWD} \leq 0.01\%$ | $\dot{x}_{LHW} = p^{31}_{LHW}, \dot{x}_{RHW} = p^{31}_{RHW},$ $\dot{x}_{FWD} = 0, \dot{x}_{AFT} = p^{31}_{AFT}$ | $p^{31}_{LHW} = -p^{True}_{LHW} \cdot L_{EngLH} + p^{True}_{AFT}$ $p^{31}_{RHW} = -p^{True}_{RHW} \cdot L_{EngRH}$ $p^{31}_{AFT} = -p^{True}_{AFT}$ |
| 32 | $z_{LHW} \geq 70\% \wedge$ $z_{RHW} < 70\% \wedge$ $z_{FWD} \leq 0.01\%$ | $\dot{x}_{LHW} = p^{32}_{LHW}, \dot{x}_{RHW} = p^{32}_{RHW},$ $\dot{x}_{FWD} = 0, \dot{x}_{AFT} = p^{32}_{AFT}$ | $p^{32}_{LHW} = -p^{True}_{LHW} \cdot L_{EngLH}$ $p^{32}_{RHW} = -p^{True}_{RHW} \cdot L_{EngRH} + p^{True}_{AFT}$ $p^{32}_{AFT} = -p^{True}_{AFT}$ |
| 40 | $z_{FWD}, z_{AFT} \leq 0.01\%$ | $\dot{x}_{LHW} = p^{40}_{LHW}, \dot{x}_{RHW} = p^{40}_{RHW},$ $\dot{x}_{FWD} = \dot{x}_{AFT} = 0$ | $p^{40}_{LHW} = -p^{True}_{LHW} \cdot L_{EngLH}$ $p^{40}_{RHW} = -p^{True}_{RHW} \cdot L_{EngRH}$ |

**Table 3.** Triggering conditions of fuel stages (FS) and true pump rates during the defueling sequence which forms the fuel system state function $f$

| Tank | True Pump Rate |
|---|---|
| Pump Rate dependency on tank content | $\frac{\partial p_{LHW}}{\partial x_{LHW}} = \frac{\partial p_{RHW}}{\partial x_{RHW}} = 50\frac{s}{\mu g \cdot kg}, \frac{\partial p_{FWD}}{\partial x_{FWD}} = \frac{\partial p_{AFT}}{\partial x_{AFT}} = 66.7\frac{s}{\mu g \cdot kg}$ $p_{0,LHW} = 0.55,\ p_{0,RHW} = 0.45,\ p_{0,FWD} = 0.30,\ p_{0,AFT} = 0.35$ |
| Pump Rate dependency on fuel inclination angle | $\frac{\partial p_{LHW}}{\partial \tau_{LHW}} = \frac{\partial p_{RHW}}{\partial \tau_{RHW}} = \frac{\partial p_{FWD}}{\partial \tau_{FWD}} = \frac{\partial p_{AFT}}{\partial \tau_{AFT}} = 3.5\frac{kg}{s}$ |
| Basic pump rate inaccuracy | $F_{1,LHW} = F_{1,RHW} = F_{1,FWD} = F_{1,AFT} = \pm 0.015\ kg/s$ |
| Parameters for $F_2$ valid for all tank | $l_1 = 1 \cdot \left(kg/s\right)^2, l_2 = 0.01, \sigma_\tau = 25°$ |
| Distribution factor of fuel to left and right wing tanks | $\lambda_{LH} = \frac{1}{2} + 0.02\frac{x_{LHW} - x_{RHW}}{x_{LHW}^{\max}}, \lambda_{RH} = 1 - \lambda_{LH}$ |

**Table 4.** Pump rate characteristics

| $k_1$ | $k_2$ | $k_3$ | $\sigma_1$ | $\sigma_2$ | $\sigma_3$ | $\sigma_4$ |
|---|---|---|---|---|---|---|
| 50kg | 0.05 | 0.01 | 0.3kg | 5kg/s | 0.4 | 20m/s² |

**Table 5.** Parameters of the measurement noise $G \cdot v$

| OE | $\Delta x_{LHW}$ | $\Delta x_{RHW}$ | $\Delta x_{FWD}$ | $\Delta x_{AFT}$ | $\Delta x_{CG}$ | $\Delta y_{CG}$ |
|---|---|---|---|---|---|---|
| **Min Value S&L** | -272 kg | -263 kg | 0 kg | 0 kg | -0.208 m | -0.004 m |
| **Max Value S&L** | 240 kg | 241 kg | 283 kg | 583 kg | 0.073 m | 0.005 m |
| **RMS Value S&L** | ±108 kg | ±105 kg | ±142 kg | ±290 kg | ±0.082 m | ±0.002 m |
| **Min Value MAN** | -261 kg | -235 kg | 0 kg | 0 kg | -0.310 m | -0.132 m |
| **Max Value MAN** | 374 kg | 392 kg | 410 kg | 843 kg | 0.084 m | 0.142 m |
| **RMS Value MAN** | ±144 kg | ±146 kg | ±186 kg | ±373 kg | ±0.101 m | ±0.017 m |

**Table 6.** Deviations of tank contents and cg data from the true values for the output error approach (OE) during straight and level flight (S&L) and maneuvering (MAN)

| SOE | $\Delta x_{LHW}$ | $\Delta x_{RHW}$ | $\Delta x_{FWD}$ | $\Delta x_{AFT}$ | $\Delta x_{CG}$ | $\Delta y_{CG}$ |
|---|---|---|---|---|---|---|
| **Min Value S&L** | -10 kg | 0 kg | 0 kg | 0 kg | -0.019 m | 0 m |
| **Max Value S&L** | 54 kg | 105 kg | 67 kg | 58 kg | 0.021 m | 0.019 m |
| **RMS Value S&L** | ±31 kg | ±62 kg | ±36 kg | ±29 kg | ±0.01 m | ±0.01 m |
| **Min Value MAN** | 0 kg | 0 kg | 0 kg | 0 kg | -0.093 m | -0.042 m |
| **Max Value MAN** | 109 kg | 147 kg | 217 kg | 269 kg | 0.053 m | 0.053 m |
| **RMS Value MAN** | ±72 kg | ±97 kg | ±97 kg | ±106 kg | ±0.024 m | ±0.01 m |

**Table 7.** Deviations of tank contents and cg data from the true values for the stabilized output error approach (SOE) during straight and level flight (S&L) and maneuvering (MAN)

| ProbeMin | $\Delta x_{LHW}$ | $\Delta x_{RHW}$ | $\Delta x_{FWD}$ | $\Delta x_{AFT}$ | $\Delta x_{CG}$ | $\Delta y_{CG}$ |
|---|---|---|---|---|---|---|
| **Min Value S&L** | -152 kg | -150 kg | -98 kg | -157 kg | -0.029 m | -0.023 m |
| **Max Value S&L** | 29 kg | 29 kg | 19 kg | 20 kg | 0.025 m | 0.028 m |
| **RMS Value S&L** | ±80 kg | ±79 kg | ±40 kg | ±55 kg | ±0.008 m | ±0.004 m |
| **Min Value MAN** | -238 kg | -236 kg | -228 kg | -222 kg | -0.081 m | -0.096 m |
| **Max Value MAN** | 6 kg | 12 kg | 0 kg | 0 kg | 0.103 m | 0.066 m |
| **RMS Value MAN** | ±91 kg | ±90 kg | ±61 kg | ±75 kg | ±0.018 m | ±0.012 m |

**Table 8.** Deviations of tank contents and cg data from the true values for minimum probe values during straight and level flight (S&L) and maneuvering (MAN)

| ProbeMax | $\Delta x_{LHW}$ | $\Delta x_{RHW}$ | $\Delta x_{FWD}$ | $\Delta x_{AFT}$ | $\Delta x_{CG}$ | $\Delta y_{CG}$ |
|---|---|---|---|---|---|---|
| **Min Value S&L** | -70 kg | -87 kg | -40 kg | -28 kg | -0.018 m | -0.02 m |
| **Max Value S&L** | 68 kg | 67 kg | 70 kg | 56 kg | 0.025 m | 0.014 m |
| **RMS Value S&L** | ±30 kg | ±30 kg | ±19 kg | ±16 kg | ±0.006 m | ±0.003 m |
| **Min Value MAN** | -224 kg | -196 kg | -192 kg | -164 kg | -0.058 m | -0.083 m |
| **Max Value MAN** | 84 kg | 85 kg | 67 kg | 68 kg | 0.064 m | 0.032 m |
| **RMS Value MAN** | ±35 kg | ±35 kg | ±20 kg | ±23 kg | ±0.009 m | ±0.005 m |

**Table 9.** Deviations of tank contents and cg data from the true values for maximum probe values during straight and level flight (S&L) and maneuvering (MAN)

| ProbeMean | $\Delta x_{LHW}$ | $\Delta x_{RHW}$ | $\Delta x_{FWD}$ | $\Delta x_{AFT}$ | $\Delta x_{CG}$ | $\Delta y_{CG}$ |
|---|---|---|---|---|---|---|
| **Min Value S&L** | -93 kg | -96 kg | -59 kg | -86 kg | -0.018 m | -0.02 m |
| **Max Value S&L** | 29 kg | 29 kg | 19 kg | 20 kg | 0.02 m | 0.014 m |
| **RMS Value S&L** | ±34 kg | ±34 kg | ±15 kg | ±25 kg | ±0.004 m | ±0.002 m |
| **Min Value MAN** | -204 kg | -229 kg | -194 kg | -213 kg | -0.049 m | -0.079 m |
| **Max Value MAN** | 18 kg | 18 kg | 11 kg | 10 kg | 0.055 m | 0.034 m |
| **RMS Value MAN** | ±40 kg | ±40 kg | ±26 kg | ±34kg | ±0.009 m | ±0.005 m |

**Table 10.** Deviations of tank contents and cg data from the true values for mean probe values during straight and level flight (S&L) and maneuvering (MAN)

## 8. FIGURES

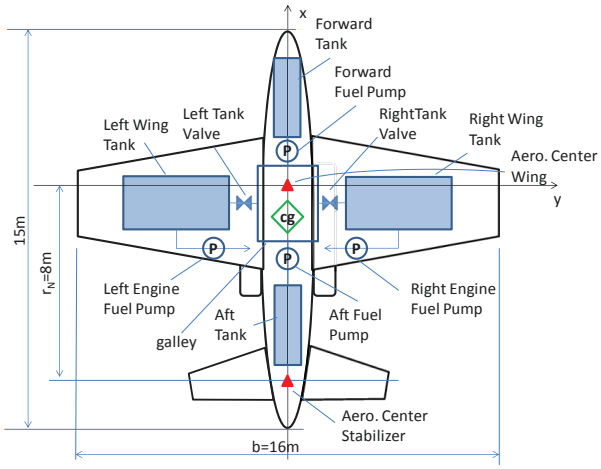


**Figure 1.** Fuel system of a generic fighter aircraft

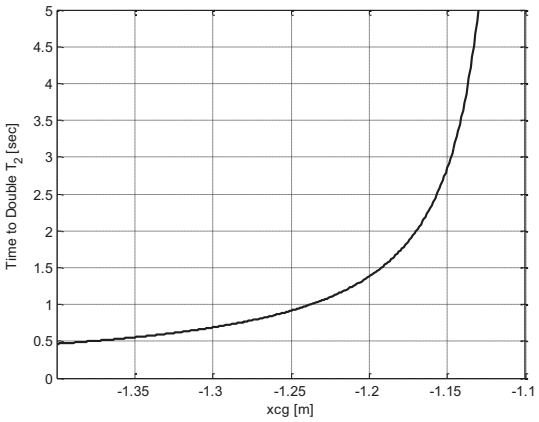


**Figure 2.** Time to double $T_2$ versus longitudinal c.g. position $x_{CG}$

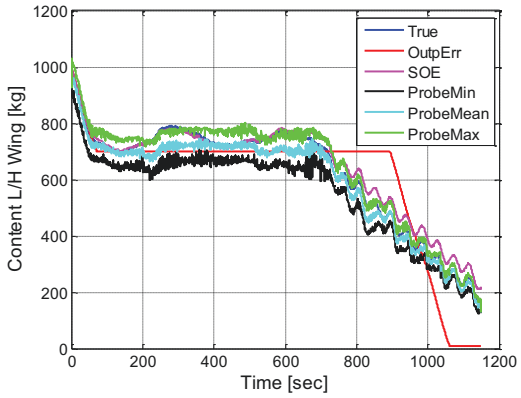


**Figure 3.** True, measured and estimated left hand wing tank content $x_{LHW}$ during S&L

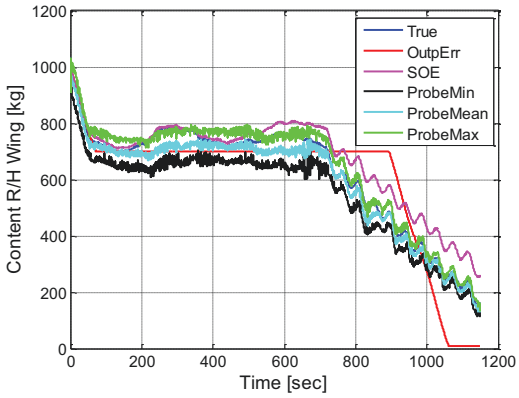


**Figure 4.** True, measured and estimated right hand wing tank content $x_{RHW}$ during S&L

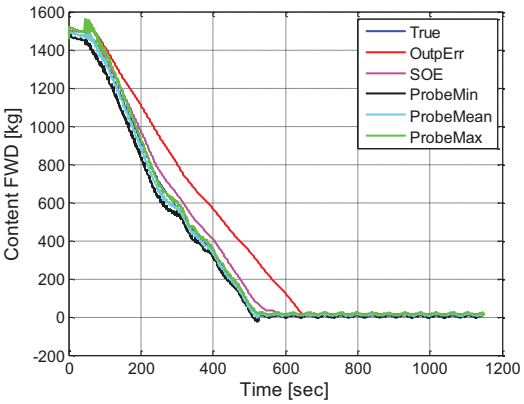


**Figure 5.** True, measured and estimated forward tank content $x_{FWD}$ during S&L

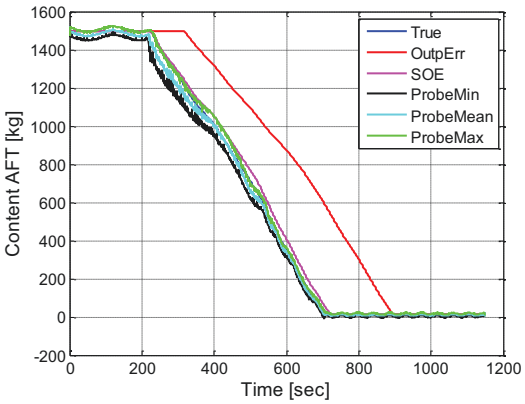


**Figure 6.** True, measured and estimated aft tank content $x_{AFT}$ during S&L

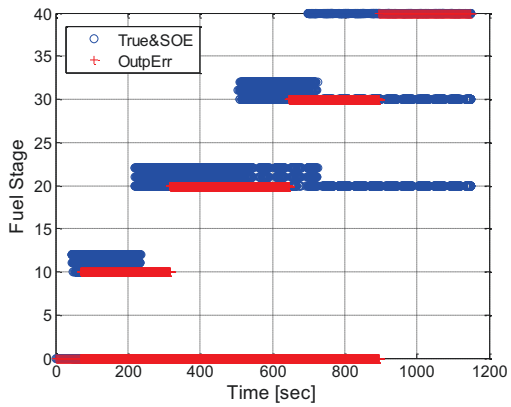


**Figure 7.** Fuel Stages FS during S&L

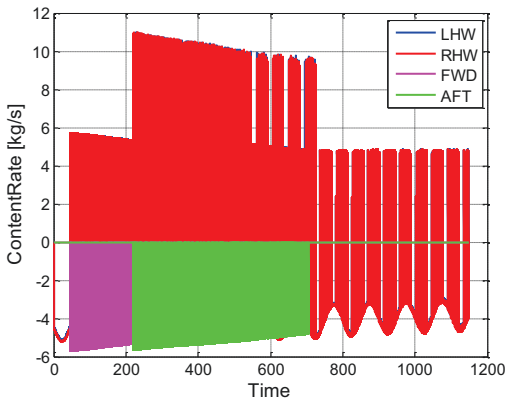


**Figure 8.** True content rate $dx_i/dt$ during S&L for all tanks

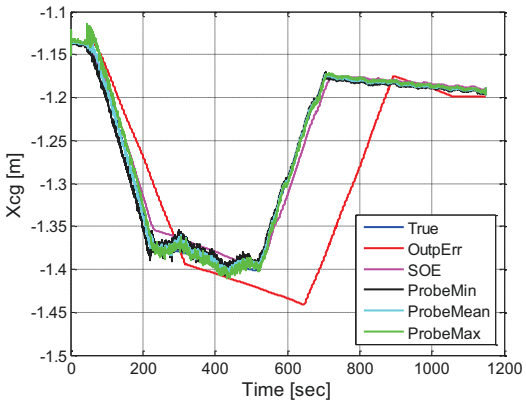


**Figure 9.** True, measured and estimated $x_{CG}$ during S&L

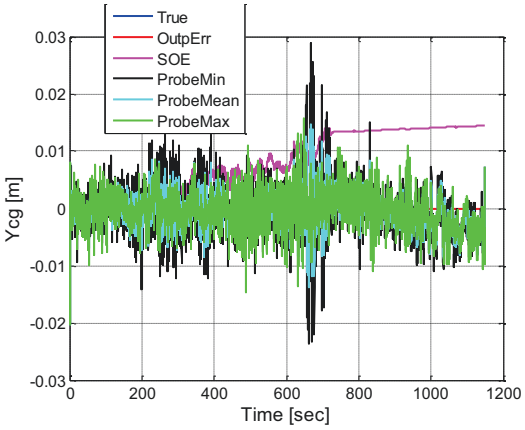


**Figure 10.** True, measured and estimated $y_{CG}$ during S&L

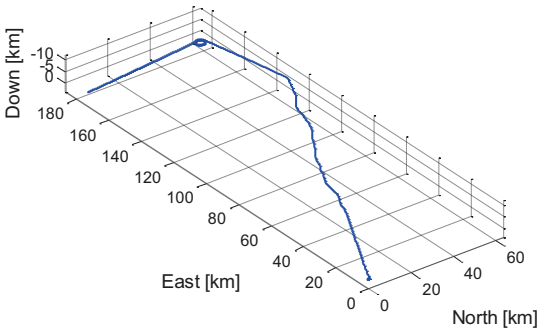


**Figure 11.** Flight path $X_E$ in earth fixed coordinates during maneuvering

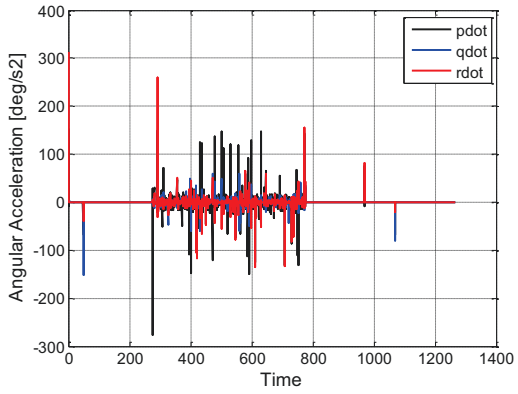


**Figure 12.** Angular accelerations (*dp/dt,dq/dt,dr/dt*) during maneuvering

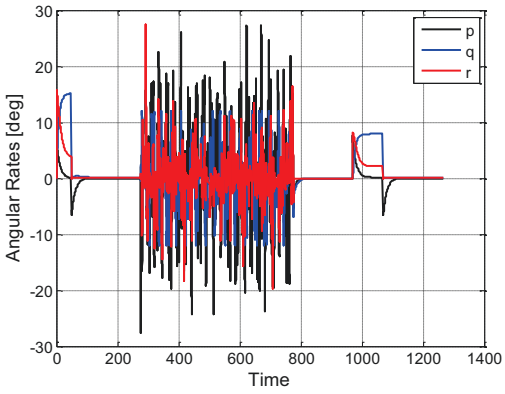


**Figure 13.** Angular rates (*p,q,r*) during maneuvering

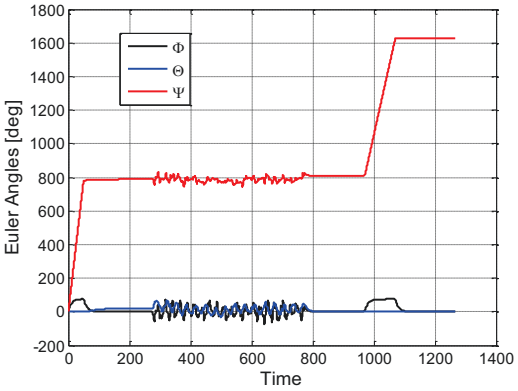


**Figure 14.** Euler angles ($\Phi,\Theta,\Psi$) during maneuvering

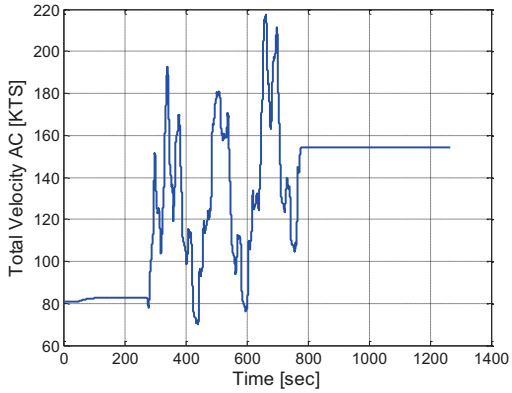


**Figure 15.** Total velocity $|V_{AC}|$ during maneuvering

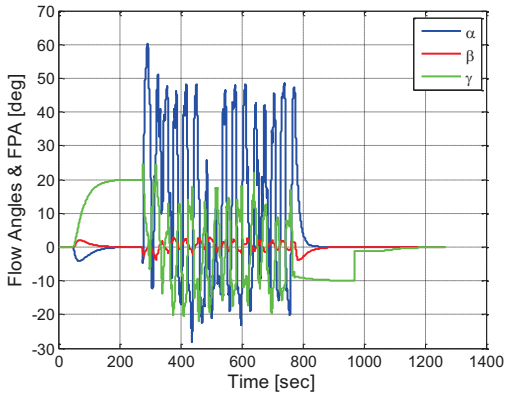


**Figure 16.** Angle of attack $\alpha$ and sideslip $\beta$ and flight path angle $\gamma$ during maneuvering

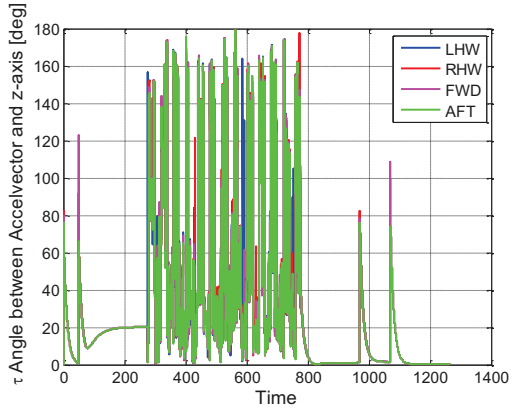


**Figure 17.** True fuel inclination angle $\tau$ during maneuvering for all tanks

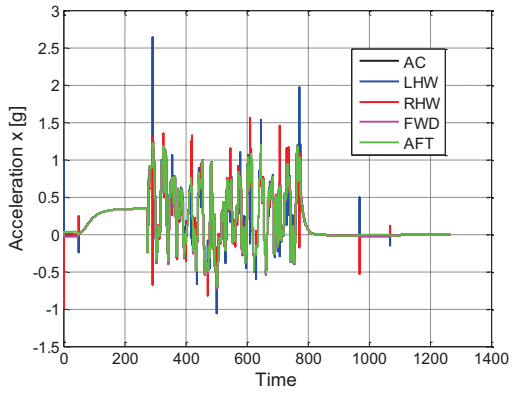


**Figure 18.** Acceleration in x-direction $A_x$ for A/C and at the tanks during maneuvering

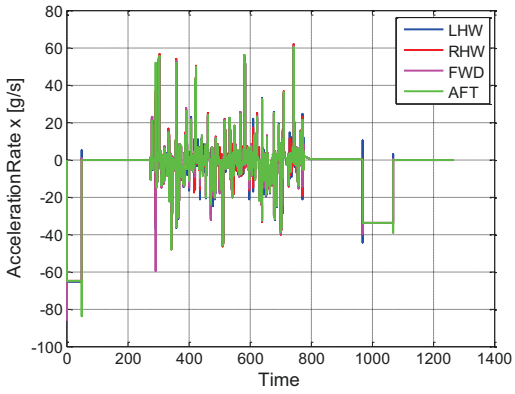


**Figure 21.** Acceleration Rate in x-direction $S_x$ for A/C and at the tanks during maneuvering

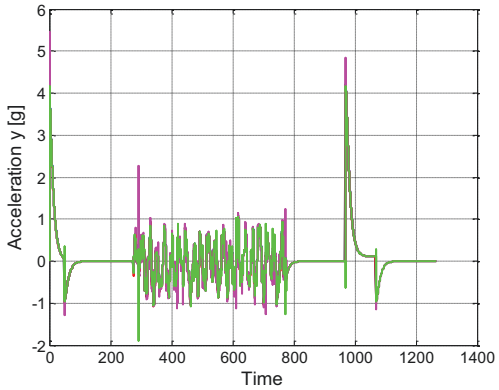


**Figure 19.** Acceleration in y-direction $A_y$ for A/C and at the tanks during maneuvering

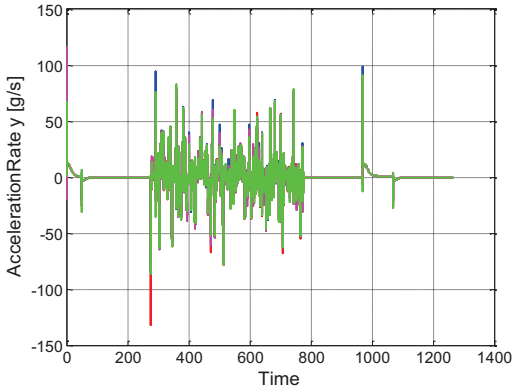


**Figure 22.** Acceleration Rate in y-direction $S_y$ for A/C and at the tanks during maneuvering

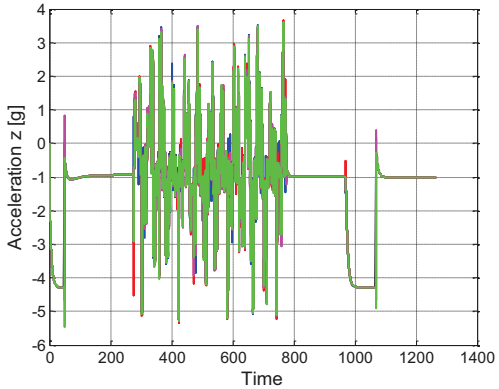


**Figure 20.** Acceleration in z-direction $A_z$ for A/C and at the tanks during maneuvering

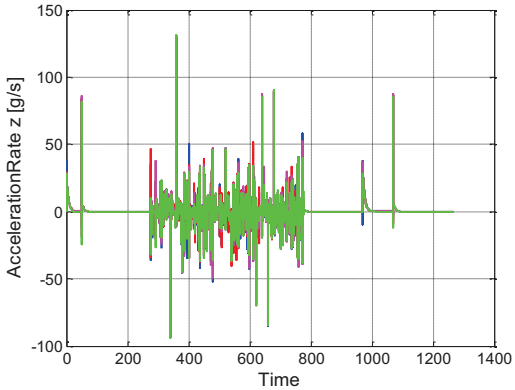


**Figure 23.** Acceleration Rate in z-direction $S_z$ for A/C and at the tanks during maneuvering

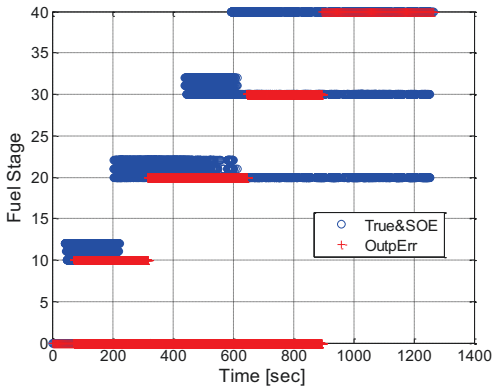


**Figure 24.** Fuel Stages FS during maneuvering

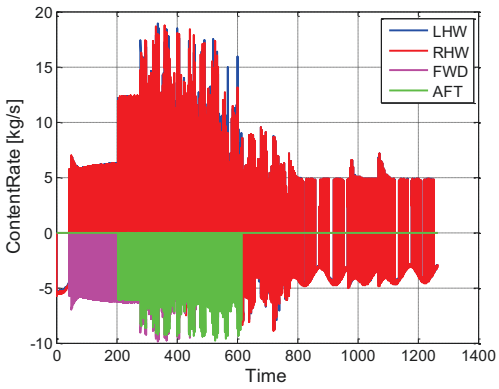


**Figure 25.** True contentrate $dx_i/dt$ during maneuvering for all tanks

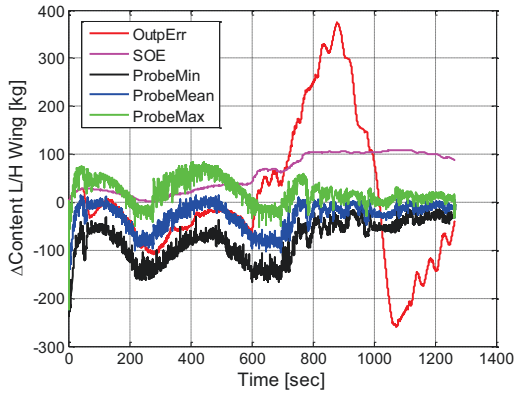


**Figure 26.** Measured and estimated left hand wing tank content deviation from true value $\Delta x_{LHW}$ during maneuvering

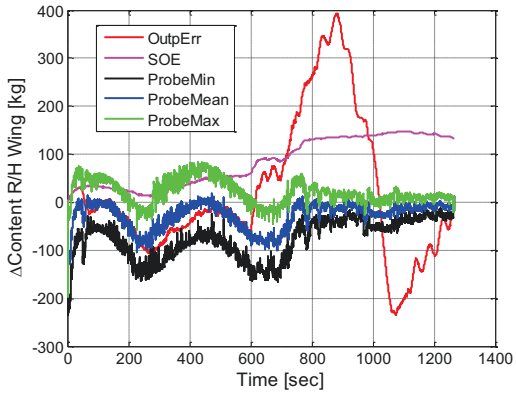


**Figure 27.** Measured and estimated right hand wing tank content deviation from true value $\Delta x_{RHW}$ during maneuvering

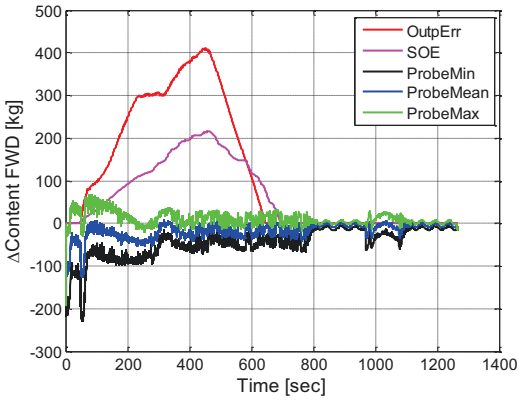


**Figure 28.** Measured and estimated forward tank content deviation from true value $\Delta x_{FWD}$ during maneuvering

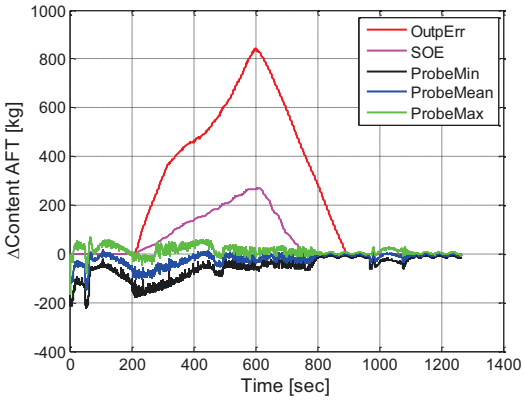


**Figure 29.** Measured and estimated aft tank content deviation from true value $\Delta x_{AFT}$ during maneuvering

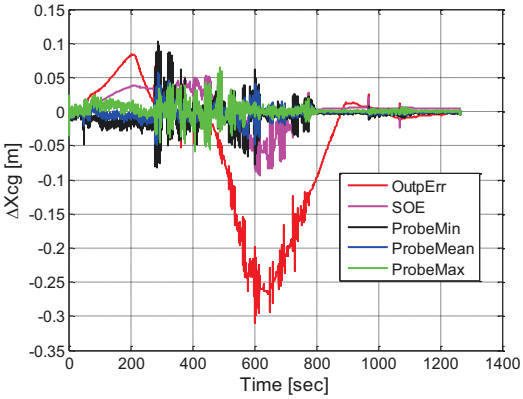


**Figure 30.** Measured and estimated longitudinal CG deviation from true value $\Delta x_{CG}$ during maneuvering

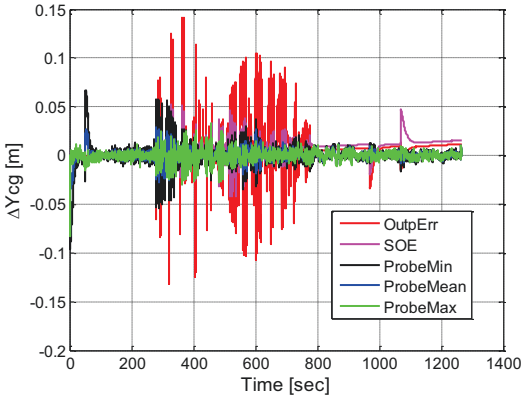


**Figure 31.** Measured and estimated lateral CG deviation from true value $\Delta y_{CG}$ during maneuvering